



Supporting Online Material for

RIM-Binding Protein, a Central Part of the Active Zone, Is Essential for Neurotransmitter Release

Karen S. Y. Liu, Matthias Siebert, Sara Mertel, Elena Knoche, Stephanie Wegener, Carolin Wichmann, Tanja Matkovic, Karzan Muhammad, Harald Depner, Christoph Mettke, Johanna Bückers, Stefan W. Hell, Martin Müller, Graeme W. Davis, Dietmar Schmitz,* Stephan J. Sigrist*

*To whom correspondence should be addressed. E-mail: dietmar.schmitz@charite.de (D.S.); stephan.sigrist@fu-berlin.de (S.J.S.)

Published 16 December 2011, *Science* **334**, 1565 (2011)
DOI: 10.1126/science.1212991

This PDF file includes

Materials and Methods
Figs. S1 to S7
References

Supporting Online Material

Materials and Methods

Genetics. All fly strains were reared under standard laboratory conditions (S1). y^1 , w^{1118} was used as background for transgenesis. Estimated cytology docking site for integration of the *drpb* genomic rescue construct was 28E7 and transgenesis was mediated by Phi31 system using P[acman] strain, PBac{yellow[+]-attP-3B}VK00002.

Generation of *drpb* deletion *Df(3R)S201*. *drpb* chromosomal deletion was constructed using the Flp recombinase system as previously described (S2). The different parental lines P{XP}d00347 and PBac{RB}Atx2e00368 were provided by the Exelixis collection at Harvard Medical School. Screening of positive candidates in deletion generation was conducted by loss of eye color and confirmed with the presence of a 1.7kb amplicon by RT-PCR. A fusion product of both parental Piggybac elements is amplified by using primers described in S2; XP5'+: 5'-AATGATTCGCAGTGGGAAGGCT-3' and RB3'+: 5'-TGCATTTGCCTTTCGCCTTAT-3'.

Chemical mutagenesis. The EMS screen was performed according to standard protocols. In brief, isogenic w^{1118} males were mutagenized with 25 mM EMS solution and crossed to virgins carrying a third chromosomal balancer. For initial mapping, male F1 offspring were crossed with *Df(3R)S201* virgins, and candidate flies were tested for adult vitality with different lines including *drpb^{Minos}*, and the genomic transgene entailing the whole *drpb* locus (*Rescue*). Genomic DNA was extracted from positive candidate flies, and PCR amplicons containing *drpb* exon clusters were double-strand sequenced to identify the mutations.

Generation of *drpb* antibodies.

anti-DRBP^{C-Term} antibody: A rabbit polyclonal antibody was raised against a synthetic peptide with the following sequence: VLSKGKDLFGKF. The specificity of the affinity-purified antibody was confirmed by immuno-fluorescence analysis of control and *drpb* mutant animals.

anti-DRBP^{N-Term} antibody: A rabbit polyclonal antibody was raised against a 6×His-tagged fusion protein with the following sequence:

MQYGTGQTSVEKLLSGTSGITGIPPLPVNIHTMKAMPTALSQRGTIQLYNLQSTTMPLLSL
NSHNLPPAGSTSYSALGAGGGTSLTHPTMANLGLLDTGTLGSLGSLGSGVGGITG
ATSLYGLSGGGGAGGLGSSYGPPFLDVASSASYPFTAAALRQASKMKMLDEIDIPLTR
YNRSSPCSPIPPNNWGLDEFDGLSVSMMHNRGGLALGALDLDTRNHGLNGASEPQVD
MLDIPG

The fragment for expression was amplified from *drbp* cDNA clone AT04807 (*Drosophila* Genomics Resource Center) using primers: Fw: 5'-CACCATGCAGTACGGAACCGGACAG-3' and Rv: 5'-CTATCCAGGAATATCGAGCATATC-3' and TOPO cloned into pENTR D-TOPO. For expression, the sequence was then transferred to pDEST17 with a Gateway reaction and expressed in *Escherichia coli* and purified using a protocol including denaturing and refolding of the protein. The antibody containing serum was affinity purified versus the same protein as used for immunization.

Immunostainings. Dissection and immunostainings were performed as described before (S3). All larvae were raised at 25°C on semi-defined medium (Bloomington recipe) and the following genotypes were used: Control: +/+ (*w¹¹¹⁸*) (everything except Fig. 4F where control was: OK6-Gal4/+; UAS *Cac^{GFP}*/+); *drbp^{Minos}*: Mi{ET1}*CG43073^{MB02027}/Df(3R)S201* (everything except Fig. 4F where *drbp^{Minos}* was: OK6-Gal4, UAS *Cac^{GFP}* /+; Mi{ET1}*CG43073^{MB02027}/Df(3R)S201*); *drbp^{STOP1}*: *drbp^{STOP1}/Df(3R)S201* (everything except Fig. 4F where *drbp^{STOP1}* was: OK6-Gal4, UAS *Cac^{GFP}* /+; *drbp^{STOP1}/Df(3R)S201*); *drbp^{STOP2}*: *drbp^{STOP2}/Df(3R)S201*; *drbp^{STOP3}*: *drbp^{STOP3}/Df(3R)S201*; Rescue: *drbp* 50kb BAC, *sco*/+; *drbp^{STOP1}/Df(3R)S201*; *brp^{1.3}*: *brp^{1.3}/Df(2R)BSC29*; *brp⁶⁹*: *brp⁶⁹/Df(2R)BSC29*.

Primary antibodies were used in the following concentrations: mouse monoclonal Nc82 anti-BRP^{C-Term} antibody 1:250 (provided by E. Buchner), mouse monoclonal 3E6 anti-GFP antibody 1:500, rabbit anti-DGluRIID 1:500 (S3), rabbit antiRBP^{C-Term} 1:500, rabbit antiRBP^{N-Term} 1:100.

Except for staining with anti-GFP, where larvae were fixed for 5 min with ice-cold ethanol, all fixations were performed for 10 min with 4 % paraformaldehyde (PFA) in 0.1 mM phosphate buffered saline (PBS).

Secondary antibodies for standard immunostainings were used in the following concentrations: goat anti-HRP-Cy5 1:200; goat anti-rabbit-Cy3 1:500, goat anti-mouse Alexa Fluor-488 1:500.

Secondary antibodies for STED were used in the following concentrations: goat anti-mouse Atto594 1:250, goat anti-rabbit Atto594 1:250, goat anti-mouse Atto647N 1:100, goat anti-rabbit Atto647N 1:100.

Imaging acquisition and analysis. Image acquisition and processing was performed as previously described (S4). Images from fixed samples were taken from the 3rd instar larval NMJ (segments A3, A4) of either muscles 6 and 7 (Fig. 2B) or muscle 4 (everything else). Images for figures were processed with ImageJ software to enhance brightness using the brightness/contrast function and smoothed (1-2 Pixel Sigma radius) using the Gauss blur function. Quantifications of AZ number, NMJ size, and Cac^{GFP} intensity were performed as previously described (S5). Further details on imaging and data processing are available on request. Data were analyzed using the Mann-Whitney U test for linear independent data groups. Means are annotated \pm SEM. Asterisks are used to denote significance: *, $P < 0.05$; **, $P < 0.01$; ***, $P < 0.001$; n.s. (not significant), $P > 0.05$).

STED microscopy. 2-color STED images were recorded with a custom-built STED-microscope which combines two pairs of excitation and STED laser beams all derived from a single supercontinuum laser source (as described in S6). STED images were processed using a linear deconvolution function integrated into Inspector Software. The point spread function (PSF) for deconvolution was generated by using a 2D Lorentz function with its half-width and half-length fitted to the half-width and half-length of each individual image. Distance measurements (Fig. 1F) were performed on deconvoluted, merged images. A line profile was laid across vertical oriented synapses and the peak to peak distance measured. A mean value was acquired over 25 synapses and the standard deviation corrected for the approx. 10 nm deviation between the 2 channels using the formula: $(SD^2+100)^{-2}$.

Electron microscopy. Conventional embedding, HPF/FS and immuno-EM were performed as described previously (S7). For electron-tomography, 250 nm conventional embedded sections were applied to Formvar-coated copper 100 mesh grids and stained with 4% uranyl acetate and Reynold's lead citrate. Five-nanometer gold beads were applied on both sides of the grid. A double tilt series was acquired at a JEOL JEM 2100 at 200 kV from -55° to $+55^\circ$ with 1°

increment using Serial EM. Reconstruction and rendering was done using the IMOD software package.

Electrophysiology. TEVC recordings were performed at room temperature on male, 3rd instar, larval NMJs (muscle 6, segments A2, A3) essentially as previously reported (S8). The composition of the extracellular haemolymph-like saline (HL-3) (S9) was (in mM): NaCl 70, KCl 5, MgCl₂ 20, NaHCO₃ 10, trehalose 5, sucrose 115, HEPES 5, CaCl₂ as indicated, pH adjusted to 7.2. Recordings were made from cells with an initial V_m between -50 and -70 mV, and input resistances of ≥ 4 M Ω , using intracellular electrodes with resistances of 8-20 M Ω , filled with 3 M KCl. eEJCs, which reflect the compound EJC of both motoneurons innervating muscle 6, and mEJCs were recorded at -60 mV and -80 mV, respectively. Signals were digitized at 10 kHz and low-pass filtered at 1 kHz. The quantal content was estimated by dividing the average eEJC amplitude through that of the average mEJC, recorded from the same cell. Miniature EJC recordings lasted for 90 s, paired-pulse recordings consisted of 10 traces/ interval/ cell, and 0.2 Hz stimulation protocols included 20 traces/ cell. High-frequency stimulation followed 30 s rest. During paired pulse stimulation, 4 s rest were left between paired-pulses. The amplitude of the 2nd pulse in 10 ms ISI paired-pulse recordings was measured from the peak to the point of interception with the extrapolated 1st pulse. The rise time and decay time constant (τ) were obtained from the average event of the respective recording. The rise time was measured from 10 to 90 % of the maximum amplitude, and the decay was fit with a single exponential function from 60 % of the peak. The amplitudes of the five pulses high-frequency stimulation with 10 ms ISI were determined as the difference between the peak value of the EPSC and the baseline value before onset of that EPSC. The recordings were analyzed with pClamp 10 and MATLAB R2010b. Stimulation artifacts of eEJCs were removed for clarity. The data are reported as mean \pm SEM, n indicates the number of cells examined. In the figures, the level of significance is marked with asterisks: * $P \leq 0.05$; ** $P \leq 0.01$; *** $P \leq 0.001$.

Calcium Imaging. Third instar larvae were dissected and incubated in ice cold Ca²⁺-free HL3 containing 5 mM Oregon-Green 488 BAPTA-1 (hexapotassium salt) and 1 mM Alexa 568. The nerves projecting to muscles 6/7 were cut in the presence of the dyes.

After incubation for 10 minutes, the preparation was washed with ice cold HL3 for 10 – 15 minutes. The intraterminal Ca²⁺ indicator concentration (~ 50 μ M) was approximated by

comparing the intraterminal Alexa 568 fluorescence intensity with a calibration curve obtained from measuring Alexa 568 fluorescence intensity of known Alexa 468 concentrations (dissolved in HL3) in small quartz glass cuvettes (VibroCom). Single action-potential evoked Ca^{2+} transients were measured in 1b boutons synapsing onto muscle 6/7 of segments A2/A3 at an extracellular $[\text{Ca}^{2+}]$ of 1 mM using a confocal laser-scanning system. Excitation light (488 nm) was focused onto the specimen using a 60x objective (1.0 NA), and emitted light was detected with a gallium arsenide phosphide-based photocathode photomultiplier tube. Line scans across single boutons were made at a frequency of 313 Hz. Fluorescence changes during line scans were quantified as $\Delta F/F = (F(t) - F_{\text{baseline}}) / (F_{\text{baseline}} - F_{\text{background}})$, where $F(t)$ is the fluorescence in a region of interest (ROI) containing a bouton at any given time, F_{baseline} is the mean fluorescence from a 300-ms period preceding the stimulus, and $F_{\text{background}}$ is the background fluorescence from an adjacent ROI without any indicator-containing cellular structures. The decay of the Ca^{2+} transients was fit with an exponential function. Experiments in which the resting fluorescence decreased by $> 15\%$, and/or which had a $F_{\text{baseline}} > 650$ a.u. were excluded from analysis. Data were analyzed using custom-written routines in Igor Pro 6.22.

Molecular cloning. Yeast-2-Hybrid constructs for *drbp* and *cac* were obtained by PCR using the corresponding cDNA as template (*cac* cDNA was provided by R.W. Ordway, The Pennsylvania State University, Philadelphia, PA; *drbp* cDNA clone AT04807 received through the *Drosophila* Genomics Resource Center) and cloned into the bait vector pGBKT7 or the prey vector pGADT7 using the restriction sites introduced with PCR primers. For the *drim* construct, total RNA of adult fly heads (strain *w¹¹¹⁸*) was extracted and transcribed into random hexamer-primed cDNA using the Superscript III kit.

Molecular cloning in detail.

***drbp* genomic rescue construct:**

BAC clone CH321-59F24 (genomic region 11161593-11262853), obtained from CHORI-321 library of BACPAC Resource Center (BPRC) was used as template for cloning and recombination events. Left homology arm (LA) flanked by AscI-NotI was produced by PCR using primers: 5'-AGACGGCGCGCCAGGCGGCAGGTCCTTCAGAT-3' and 5'-

AGTCGCGGCCGCATCCTCGAGAGTGGCATTGA-3'; Right homology arm (RA) flanked by NotI-PacI was produced by PCR using primers:

5'- AGTCGCGGCCGCTGCGACAGTAGCTAGCAAGA-3'

and 5'- AGACTTAATTAAGTCAATTCTGCGCCGACAA-3'.

The PCR products of LA and RA were cut by NotI and ligated to produce LARA. LARA was cut and ligated into attB-P[acman]-ApR vector using AscI-PacI. Recombination event between the BAC and attB-P[acman]-LARA-ApR entailing the complete *drbp* locus (genomic region 11193728 - 11230728) was completed as previously described (S10).

pENTER and pGADT7/pGBKT7 cloning.

All final plasmids of pENTER, pGADT7 or pGBKT7 constructs were double-strand sequenced before any further use including Gateway recombination with destination vectors.

pGADT7 DRBP SH3-I (aa 311– 483):

Primers: 5'-GCAGTCCCATGGATTCCGCCGAACAACACTGG-3' and

5'-CAAGAGGATCCTTATCACGATCCGTCCTCGGCATCG-3'; cut and ligated into pGADT7 using NcoI-BamHI.

pGADT7 DRBP FNIII (aa 508– 907):

Primers: 5'-GCAGTCCCATGGGAGGATCTGGCACGCTTA-3' and

5'-CAAGAGAATTCTGGTTGGCCTGGCTGATA-3'; cut and ligated into pGADT7 using NcoI-EcoRI.

pGADT7 DRBP SH3-II (aa 1024– 1185):

Primers: 5'-GCAGTCCCATGGCCACGAGGACCGCTCAAT-3' and

5'-CAAGAGAATTCCACGTTGCGCATGCTCTG-3'; cut and ligated into pGADT7 using NcoI-EcoRI.

pGADT7 DRBP SH3-III (aa 1138– 1307):

Primers: 5'-GCAGTCCCATGGGACACCACCGCCTCCATG-3' and

5'-CAAGAGAATTCTCCGGGCATCATGTTGTCA-3'; cut and ligated into pGADT7 using NcoI-EcoRI.

pGADT7 DRBP SH3-II+III (aa 1024– 1307):

Primers: 5'-GCAGTCCCATGGCCACGAGGACCGCTCAAT -3' and 5'-CAAGAGAATTCTCCGGGCATCATGTTGTCA-3'; cut and ligated into pGADT7 using NcoI-EcoRI.

pENTER DRBP SH3-II+III (aa 1024– 1273):

Primers: 5'-GCAGACTAGTCCACGAGGACCGCTCAAT-3' and 5'-CAAGGGCACCCGGACCCATCTGGTTGTT-3'; cut and ligated into pENTER using SpeI-KpnI.

pGBKT7 and pENTER CAC C-term (aa 1,420–1,848):

Primers: 5'-GATGCCATGGCGTTATTCGCTTTGATTCGTGA-3' and 5'-GATGCTCGAGAGCACCAATCCTCCTCATCCGAA-3'; cut and ligated into pENTER (S7) using NcoI-XhoI and into pGBKT7 using NcoI-Sall.

pGBKT7 CAC C-term D80aa (aa 1,420–1,768):

Primers: 5'-GATGCCATGGCGTTATTCGCTTTGATTCGTGA-3' and 5'-GTCTGGATCCTTATCACAGGCGATCGCGATCCCTAT-3'; cut and ligated into pGBKT7 using NcoI-BamHI.

pGBKT7 CAC C-term D160aa (aa 1,420–1,688):

Primers: 5'-GATGCCATGGCGTTATTCGCTTTGATTCGTGA-3' and 5'-GTCTGTGCGACTTATCAGCGTCTTCCGATTCCGGCTCT-3'; cut and ligated into pGBKT7 using NcoI-Sall.

pGBKT7 CAC C-term with mutation of PxxP motifs (prolines to alanines):

Three different constructs were generated by using the QuickChange Site-Directed Mutagenesis Kit, pGADT7 CAC C-term as template, and the following primer pairs: 5'-CATGGCAACAGTCATGCGCGGTATGCAGGAGGTTTCATGGTCA-3' and 5'-TGACCATGAACCTCCTGCATACCGCGCATGACTGTTGCCATG-3' for pGADT7 CAC C-term¹⁵⁹⁵ARYA;

5'-AATCGGAAGACGCCTTGCTCCGACTGCCAGTAAACCGTCAACAC-3' and
5'-GTGTTGACGGTTTACTGGCAGTCGGAGCAAGGCGTCTTCCGATT-3' for pGADT7
CAC C-term¹⁶⁹⁰APTA;
5'-GCCTTCCTCCGACTGCCAGTAAAGCGTCAACACTGCAGCTCA-3' and
5'-TGAGCTGCAGTGTTGACGCTTACTGGCAGTCGGAGGAAGGC-3' for pGADT7 CAC
C-term¹⁶⁹³ASKA.

pENTR-D DRIM PXXP:

Primers: 5'-CACCGGCTATCGGAGCACCAGTC-3' and 5'-GCTGACCACCGACTCCATG-3'
were used to amplify a 516 bp fragment from random hexamer-primed w¹¹¹⁸ cDNA. The PCR
product was cloned into pENTR-D/Topo.

pGBKT7 DRIM PXXP (aa 1458-1630):

Primers: 5'-GTACTCATATGGGCTATCGGAGCACCAGTC-3' and
5'-GTACTGAATTC GCTGACCACCGACTCCATG-3' were used to amplify a PCR product
from pENTR-D DRIM PXXP. The PCR product was cut and ligated into pGBKT7 using NdeI-
EcoRI.

Yeast-2-Hybrid. In principle, all co-transformation experiments were conducted according to the
Yeast-2-Hybrid protocols of Clontech Laboratories using the strain AH109. To ensure the
presence of both co-transformed plasmids, the co-transformed yeast was plated on minimal
synthetic-defined/-Leu/-Trp medium plates. After growing for 2-3 d, at least 10 clones each
were analyzed on synthetic-defined/-Ade/-His/-Leu/-Trp/X- α -galactosidase medium plates to
select for positive interaction. If >90% of the clones grew and turned blue in color, this was
regarded as a positive interaction of high confidence (+++). As a positive control, pGBKT7-p53
was cotransformed with pGADT7 containing the SV40 large T antigen. Negative controls
consisted either of laminin as bait together with the prey to be tested or the corresponding bait
together with the empty prey vector.

Single cell protein interaction assay. HEK293 cells were single or co-transfected with
constructs expressing bait (MARCKS-GFP::Cac-C-Term) and/or prey (mStraw::DRBP SH3-
II+III) under CVM promotor. For transfection, lipofectamine 2000 was used following

manufacture's protocol. Fluorescent images of individual cells were obtained using a confocal system.

pdMARCKS-GFP plasmid:

Membrane targeting sequence MARCKS fused to eGFP (*S11*) (gift from Pico Caroni) sub-cloned into a CMV based Gateway destination vector via NheI and Not-1.

MARCKS-GFP::Cac-C-Term and mStraw::DRBP SH3-II+III:

pENTR-Cac-C-Term and pENTR-DRBP SH3-II+III were recombined with the pdMARCKS-GFP and pdGD-CMVntStrawberry vectors via Gateway system, respectively.

Figures

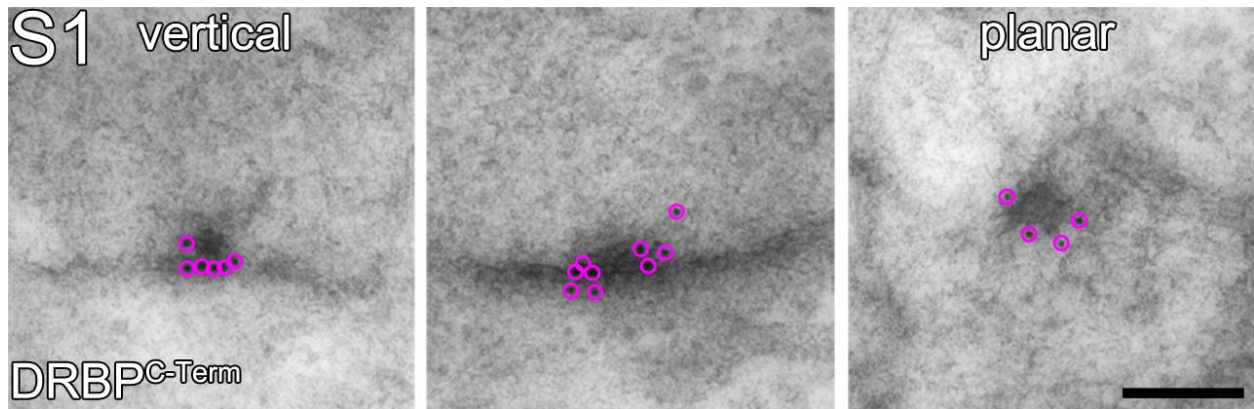
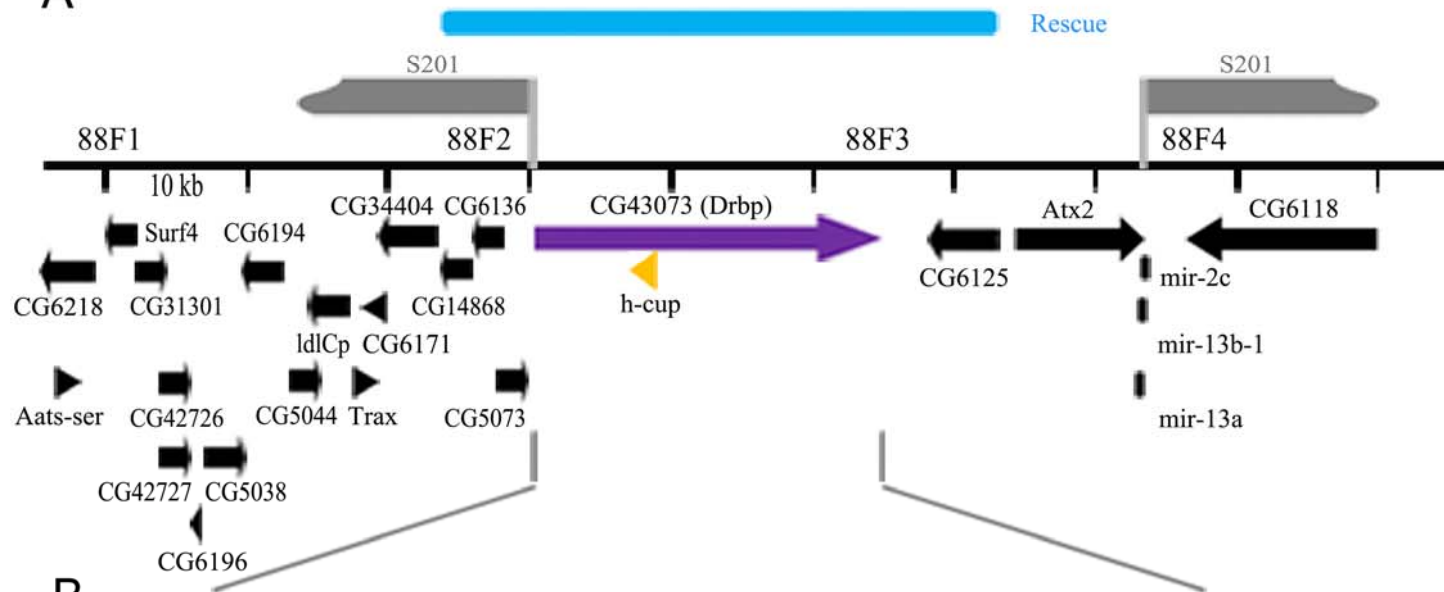


Fig. S1. Post-embedding immuno-gold labeling with DRBPC-term at larval wild-type synapses.

The vertical view shows that DRBPC-term surrounds the T-bar pedestal (left and middle panels). In a planar view DRBPC-term localizes mainly to the edges of the T-bar pedestal. Scale bar: 100 nm.

S2

A



B

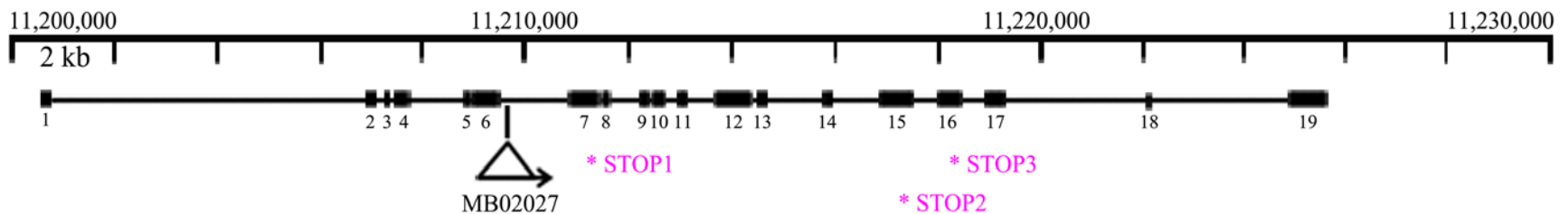


Fig. S2. Schematic representation of the *drbp* locus.

(A) Genomic region of *drbp*. *drbp* gene locus (CG43073) shown in purple. *Df(3R)S201* (here S201) breakpoints are shown in gray. *drbp* genomic rescue construct is shown in blue.

(B) Gene model of *drbp*. *drbp* encompasses 19 exons. Insertion site of MB02027 transposon (*drbp*^{Minos}) and sites of STOP codons induced in our chemical mutagenesis screen are indicated.

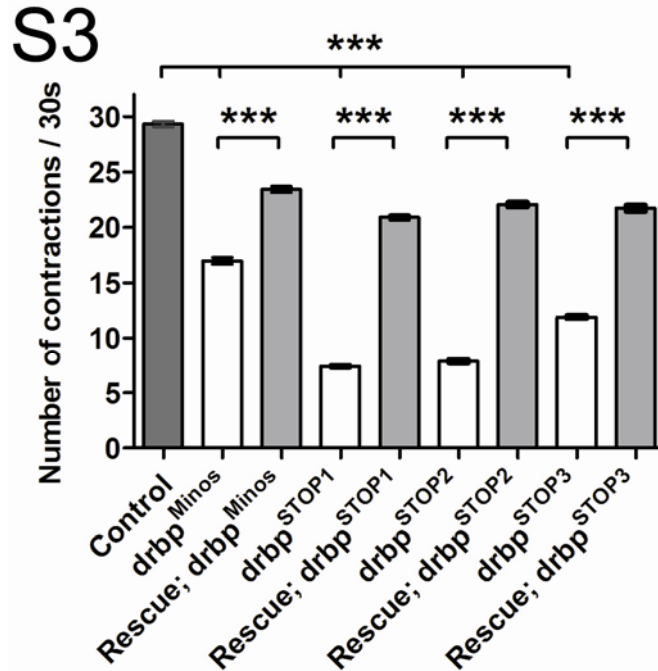


Fig. S3. Locomotion assay of *drbp* mutant larvae.

Third instar larvae of each genotype were put on an agarose plate and number of contractile motions per 30 seconds were measured (3 times for each larva, n = 45 larvae). *drbp^{Minos}* larvae moved about 50% less and *drbp^{STOP1-3}* larvae about 75% less than control larvae (control: 29.3 ± 0.3; *drbp^{Minos}*: 17.0 ± 0.3; *drbp^{STOP1}*: 7.4 ± 0.2; *drbp^{STOP2}*: 7.8 ± 0.2; *drbp^{STOP3}*: 11.9 ± 0.1; P < 0.001 compared to control; one way ANOVA with Tukey's post test). Locomotive defects could be partially rescued by introduction of one copy *drbp* genomic rescue construct (Rescue; *drbp^{Minos}*: 23.4 ± 0.3; Rescue; *drbp^{STOP1}*: 20.9 ± 0.2; Rescue; *drbp^{STOP2}*: 22.1 ± 0.2; Rescue; *drbp^{STOP3}*: 21.7 ± 0.3; P < 0.001 compared to respective *drbp* mutant, Mann-Whitney U test).

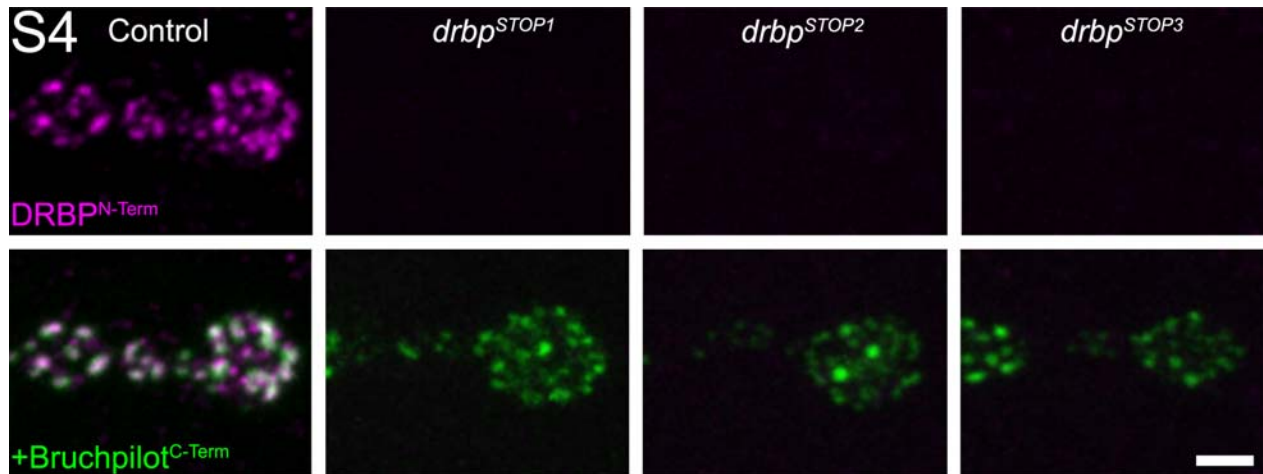


Fig. S4. *drbp* EMS mutants completely lack DRBP^{N-Term} label.

Synapses of control animals were labeled by an antibody directed against the N-Term of DRBP (magenta, merge with Bruchpilot^{C-Term} in green), whereas all *drbp* EMS mutants (*drbp*^{STOP1-3}) completely lacked the DRBP^{N-Term} signal. Scale bar: 2 μ m.

S5

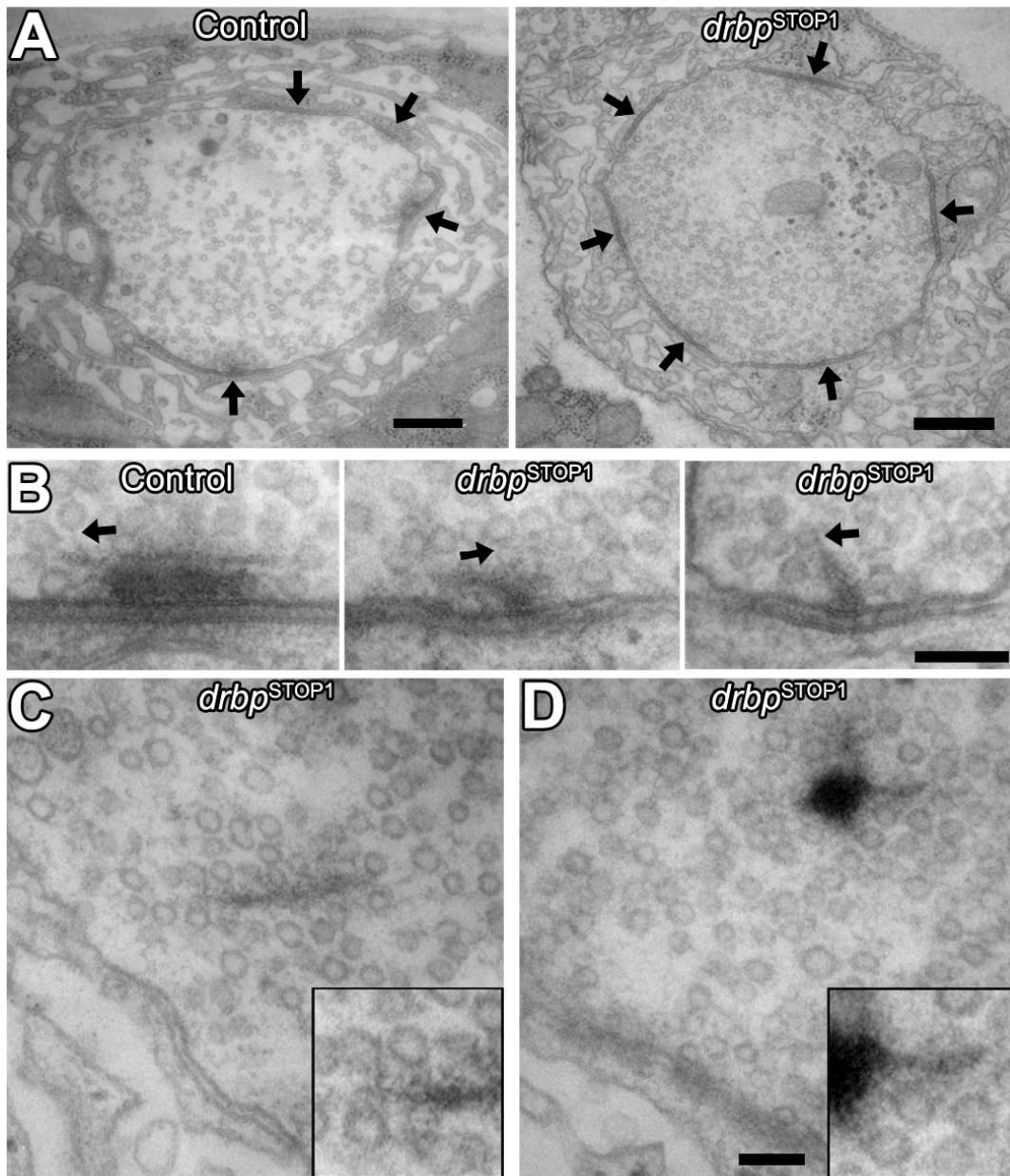


Fig. S5. Ultrastructure of conventional fixed *drbp* mutants.

(A) The overall bouton structure and number of synapses (arrows) was not altered in *drbp*^{STOP1} larvae compared to controls.

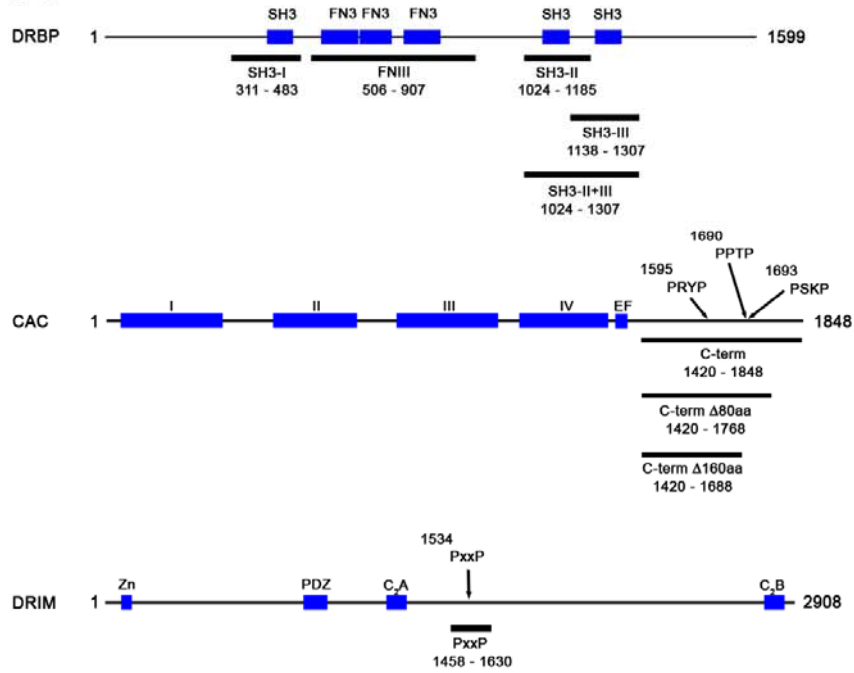
(B) Examples of abnormal electron-dense material at *drbp*^{STOP1} AZs. Arrows indicate SVs tethered to the electron-dense material.

(C, D) Floating electron-dense material in *drbp*^{STOP1} mutant presynaptic terminals. SVs appear to be attached to it (insets).

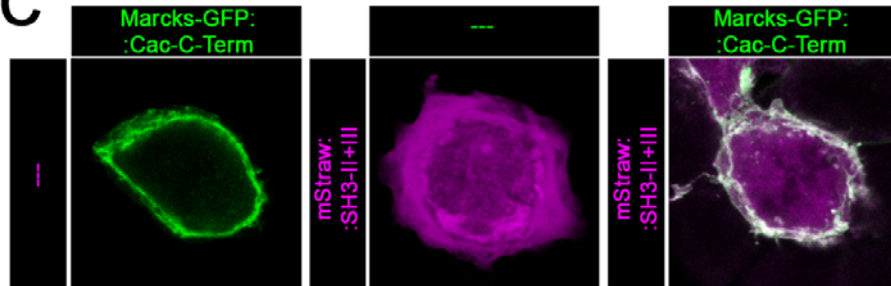
Scale bar: 500 nm (A); 100 nm (B); 75 nm (C-D).

S6

A



C



B

bait clones (pGBKT7)	prey clones (pGADT7 RBP)				
	SH3-I	FNIII	SH3-II	SH3-III	SH3-II+III
CAC C-term	-	-	-	+++	-
CAC C-term Δ80aa	-	n.d.	-	+++	-
CAC C-term Δ160aa	-	n.d.	-	-	-
CAC C-term ¹⁵⁹⁵ ARYA	-	n.d.	-	+++	-
CAC C-term ¹⁶⁹⁰ APTP	-	n.d.	-	-	-
CAC C-term ¹⁶⁹³ ASKA	-	n.d.	-	-	-
DRIM PxxP	-	-	-	+++	-

Fig. S6. DRBP SH3-III interacts with Cac C-Term and RIM in Yeast-2-Hybrid assays.

(A) Schematic of the Yeast-2-Hybrid DRBP prey and CAC and DRIM bait constructs used for co-transformation analysis. Possible interactions were tested with bait constructs containing the C-Terminal region of Cac (83% of the reported cytoplasmatic C terminus; S7) as well as truncated and PxxP motif-mutated versions of this C-Terminal region. To test interaction with DRIM only one PxxP-motif containing construct was cloned and tested. The different constructs are marked by black lines. The corresponding aa positions are indicated by numbers and the following GenBank accession numbers were used as references for DRBP (NM_169654; CG43073, variant B, 1599 aa) and DRIM (NM_001014630, 2908 aa). Blue boxes highlight different functional (e.g. SH3, PDZ, Zink-finger) or structural domains (transmembrane domains I to IV of CAC) within the proteins.

(B) PxxP motifs within the last 160 aa of CAC (¹⁶⁹⁰PPTP, ¹⁶⁹³PSKP) and the DRIM PxxP motif (aa position 1534) interact with the third SH3 domain (SH3-III) of DRBP when co-transfected into yeast. After mutagenesis of the PxxP motifs within CAC (¹⁶⁹⁰PPTP→APTA, ¹⁶⁹³PSKP→ASKA), the interaction with DRBP is lost. –, no interaction; +++, interaction of high confidence; n.d., not determined.

(C) Single cell protein interaction assay. A GFP-tagged Cac C-Term fragment is targeted to the membrane of HEK293 cells via MARCKS (green, left panel). A Strawberry-tagged DRBP SH3-II+III fragment expressed alone exhibits diffuse distribution throughout the cytoplasm (magenta, middle panel). Upon co-expression of membrane targeted Cac C-Term, the SH3-II+III fragment is translocated to the membrane (right panel).

S7

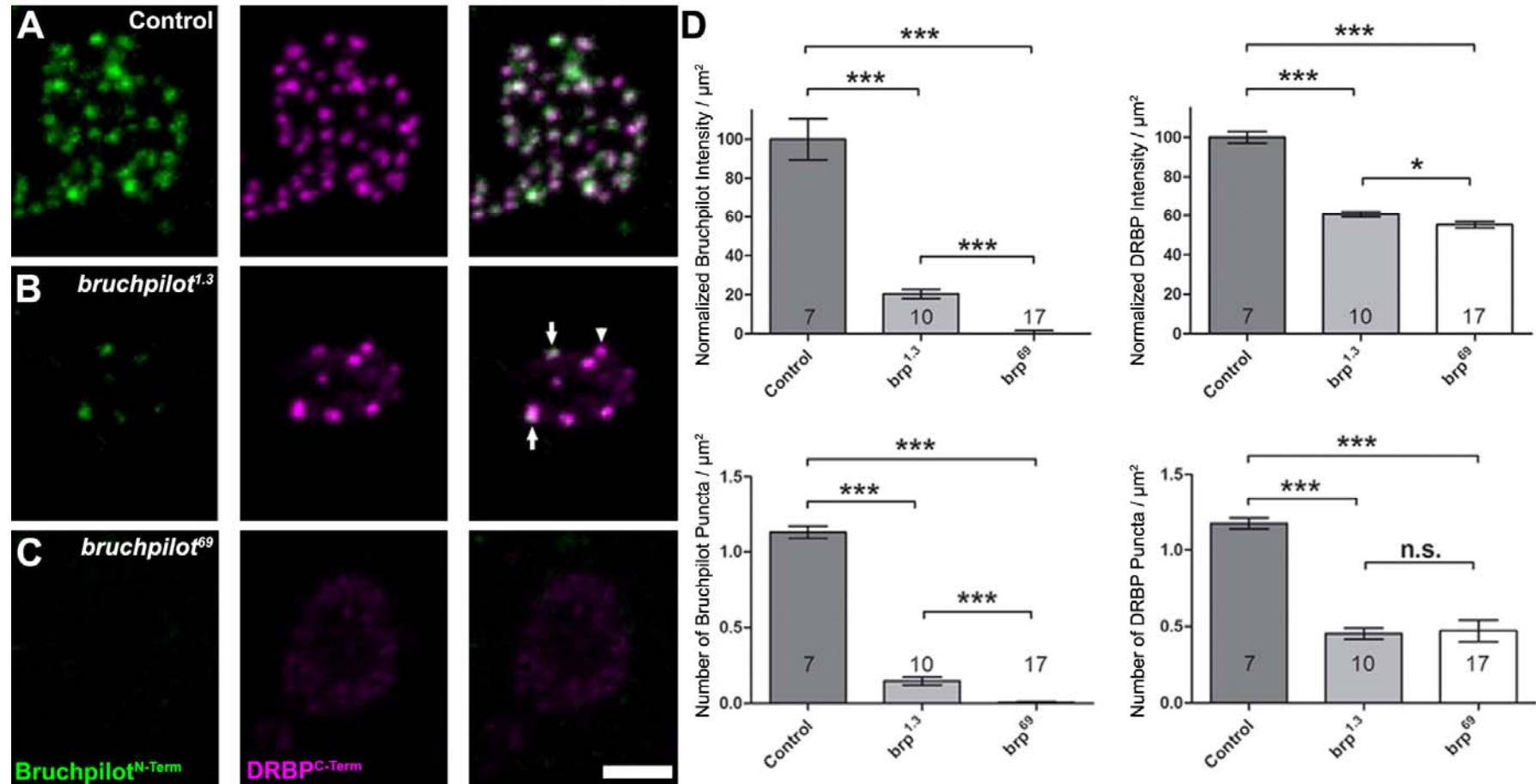


Fig. S7. DRBP localization to AZs is partially dependent on Bruchpilot.

(A) In control animals DRBP (C-Term, magenta) and Bruchpilot (N-Term, green) co-localize at every AZ.

(B) In *bruchpilot*^{1.3} mutants, which express a C-Terminally truncated version of Bruchpilot (encoding for about 70% of the full length protein), both Bruchpilot and DRBP signal intensities (Bruchpilot: control: 100% ± 10, n = 7; *brp*^{1.3}: 20% ± 2, n = 10; P = 0.0001, Mann-Whitney U test; DRBP: control: 100% ± 3, n = 7; *brp*^{1.3}: 61% ± 1, n = 10; P = 0.0001, Mann-Whitney U test; graphs in D) and number of puncta per μm^2 were reduced

(Bruchpilot: control: 1.13 ± 0.04 , $n = 7$; *brp*^{l.3}: 0.14 ± 0.03 , $n = 10$; $P = 0.0001$, Mann-Whitney U test; DRBP: control: 1.18 ± 0.04 , $n = 7$; *brp*^{l.3}: 0.45 ± 0.04 , $n = 10$; $P = 0.0001$, Mann-Whitney U test; graphs in D). All remaining Bruchpilot punctae co-localized with DRBP punctae (see arrows for examples), whereas there were some DRBP punctae without Bruchpilot counterpart (arrowhead).

(C) In *bruchpilot*⁶⁹ mutants, which completely lack Bruchpilot expression (Intensity: *brp*⁶⁹ $0\% \pm 2$, $n = 17$; $P = 0.0002$ vs control, $P < 0.0001$ vs *brp*^{l.3}, Mann-Whitney U test; number of puncta per μm^2 : *brp*⁶⁹ 0.01 ± 0.01 , $n = 17$; $P = 0.0002$ vs control, $P < 0.0001$ vs *brp*^{l.3}, Mann-Whitney U test; graphs in D), DRBP intensity is further reduced (*brp*⁶⁹ $55\% \pm 2$, $n = 17$; $P = 0.0002$ vs control, $P = 0.0372$ vs *brp*^{l.3}, Mann-Whitney U test; graphs in D), while the number of puncta per μm^2 is unchanged compared to *bruchpilot*^{l.3} mutants (*brp*⁶⁹ 0.47 ± 0.07 , $n = 17$; $P = 0.0002$ vs control, $P = 0.2380$ vs *brp*^{l.3}, Mann-Whitney U test; graphs in D). There are some boutons that completely lack distinct punctate DRBP signal of high intensity. Scale bar: 2 μm (A-C).

References

1. Y. Jin, C. C. Garner, Molecular mechanisms of presynaptic differentiation. *Annu. Rev. Cell Dev. Biol.* **24**, 237 (2008).
2. S. J. Sigrist, D. Schmitz, Structural and functional plasticity of the cytoplasmic active zone. *Curr. Opin. Neurobiol.* **21**, 144 (2011).
3. S. Schoch, E. D. Gundelfinger, Molecular organization of the presynaptic active zone. *Cell Tissue Res.* **326**, 379 (2006).
4. L. Siksou, A. Triller, S. Marty, Ultrastructural organization of presynaptic terminals. *Curr. Opin. Neurobiol.* **21**, 261 (2011).
5. R. J. Kittel *et al.*, Bruchpilot promotes active zone assembly, Ca²⁺ channel clustering, and vesicle release. *Science* **312**, 1051 (2006).
6. Y. Wang, S. Sugita, T. C. Sudhof, The RIM/NIM family of neuronal C2 domain proteins. Interactions with Rab3 and a new class of Src homology 3 domain proteins. *J. Biol. Chem.* **275**, 20033 (2000).
7. H. Hibino *et al.*, RIM binding proteins (RBPs) couple Rab3-interacting molecules (RIMs) to voltage-gated Ca(2+) channels. *Neuron* **34**, 411 (2002).
8. S. A. Spangler, C. C. Hoogenraad, Liprin-alpha proteins: Scaffold molecules for synapse maturation. *Biochem. Soc. Trans.* **35**, 1278 (2007).
9. T. Mittelstaedt, S. Schoch, Structure and evolution of RIM-BP genes: Identification of a novel family member. *Gene* **403**, 70 (2007).
10. S. W. Hell, Far-field optical nanoscopy. *Science* **316**, 1153 (2007).
11. J. Bückers, D. Wildanger, G. Vicidomini, L. Kastrup, S. W. Hell, Simultaneous multi-lifetime multi-color STED imaging for colocalization analyses. *Opt. Express* **19**, 3130 (2011).
12. J. Hou, T. Tamura, Y. Kidokoro, Delayed synaptic transmission in *Drosophila* cacophonynull embryos. *J. Neurophysiol.* **100**, 2833 (2008).
13. F. Kawasaki, R. Felling, R. W. Ordway, A temperature-sensitive paralytic mutant defines a primary synaptic calcium channel in *Drosophila*. *J. Neurosci.* **20**, 4885 (2000).
14. W. Fouquet *et al.*, Maturation of active zone assembly by *Drosophila* Bruchpilot. *J. Cell Biol.* **186**, 129 (2009).
15. F. Kawasaki, S. C. Collins, R. W. Ordway, Synaptic calcium-channel function in *Drosophila*: Analysis and transformation rescue of temperature-sensitive paralytic and lethal mutations of cacophony. *J. Neurosci.* **22**, 5856 (2002).
16. K. J. Venken, Y. He, R. A. Hoskins, H. J. Bellen, P[acman]: A BAC transgenic platform for targeted insertion of large DNA fragments in *D. melanogaster*. *Science* **314**, 1747 (2006).
17. L. Siksou *et al.*, Three-dimensional architecture of presynaptic terminal cytomatrix. *J. Neurosci.* **27**, 6868 (2007).

18. P. Rostaing, R. M. Weimer, E. M. Jorgensen, A. Triller, J. L. Bessereau, Preservation of immunoreactivity and fine structure of adult *C. elegans* tissues using high-pressure freezing. *J. Histochem. Cytochem.* **52**, 1 (2004).
19. S. Hallermann *et al.*, Naked dense bodies provoke depression. *J. Neurosci.* **30**, 14340 (2010).
20. E. O. Gracheva, E. B. Maryon, M. Berthelot-Grosjean, J. E. Richmond, Differential Regulation of synaptic vesicle tethering and docking by UNC-18 and TOM-1. *Front. Synaptic Neurosci.* **2**, 141 (2010).
21. E. Neher, T. Sakaba, Multiple roles of calcium ions in the regulation of neurotransmitter release. *Neuron* **59**, 861 (2008).
22. F. Kawasaki, B. Zou, X. Xu, R. W. Ordway, Active zone localization of presynaptic calcium channels encoded by the cacophony locus of *Drosophila*. *J. Neurosci.* **24**, 282 (2004).
23. P. S. Kaeser *et al.*, RIM proteins tether Ca²⁺ channels to presynaptic active zones via a direct PDZ-domain interaction. *Cell* **144**, 282 (2011).
24. Y. Han, P. S. Kaeser, T. C. Südhof, R. Schneggenburger, RIM determines Ca²⁺ channel density and vesicle docking at the presynaptic active zone. *Neuron* **69**, 304 (2011).
25. C. Rosenmund *et al.*, Differential control of vesicle priming and short-term plasticity by Munc13 isoforms. *Neuron* **33**, 411 (2002).
26. W. J. Jockusch *et al.*, CAPS-1 and CAPS-2 are essential synaptic vesicle priming proteins. *Cell* **131**, 796 (2007).
27. M. Bucan *et al.*, Genome-wide analyses of exonic copy number variants in a family-based study point to novel autism susceptibility genes. *PLoS Genet.* **5**, e1000536 (2009).
28. D. Pinto *et al.*, Functional impact of global rare copy number variation in autism spectrum disorders. *Nature* **466**, 368 (2010).
29. S. J. Sigrist, D. F. Reiff, P. R. Thiel, J. R. Steinert, C. M. Schuster, Experience-dependent strengthening of *Drosophila* neuromuscular junctions. *J. Neurosci.* **23**, 6546 (2003).
30. A. L. Parks *et al.*, Systematic generation of high-resolution deletion coverage of the *Drosophila melanogaster* genome. *Nat. Genet.* **36**, 288 (2004).
31. G. Qin *et al.*, Four different subunits are essential for expressing the synaptic glutamate receptor at neuromuscular junctions of *Drosophila*. *J. Neurosci.* **25**, 3209 (2005).
32. T. M. Rasse *et al.*, Glutamate receptor dynamics organizing synapse formation in vivo. *Nat. Neurosci.* **8**, 898 (2005).
33. D. Oswald *et al.*, A Syd-1 homologue regulates pre- and postsynaptic maturation in *Drosophila*. *J. Cell Biol.* **188**, 565 (2010).

34. D. Neumann, J. Bückers, L. Kastrup, S. W. Hell, S. Jakobs, Two-color STED microscopy reveals different degrees of colocalization between hexokinase-I and the three human VDAC isoforms. *PMC Biophys* **3**, 4 (2010).
35. W. Fouquet *et al.*, Maturation of active zone assembly by *Drosophila* Bruchpilot. *J. Cell Biol.* **186**, 129 (2009).
36. R. J. Kittel *et al.*, Bruchpilot promotes active zone assembly, Ca²⁺ channel clustering, and vesicle release. *Science* **312**, 1051 (2006).
37. B. A. Stewart, H. L. Atwood, J. J. Renger, J. Wang, C. F. Wu, Improved stability of *Drosophila* larval neuromuscular preparations in haemolymph-like physiological solutions. *J. Comp. Physiol. A Neuroethol. Sens. Neural Behav. Physiol.* **175**, 179 (1994).
38. K. J. Venken, Y. He, R. A. Hoskins, H. J. Bellen, P[acman]: A BAC transgenic platform for targeted insertion of large DNA fragments in *D. melanogaster*. *Science* **314**, 1747 (2006).
39. V. De Paola, S. Arber, P. Caroni, AMPA receptors regulate dynamic equilibrium of presynaptic terminals in mature hippocampal networks. *Nat. Neurosci.* **6**, 491 (2003).